ANNALS OF MEDICINE
2025, VOL. 57, NO. 1, 2431606
https://doi.org/10.1080/07853890.2024.2431606

RESEARCH ARTICLE

OPEN ACCESS Check for updates

Machine learning-based radiomic features of perivascular adipose tissue in coronary computed tomography angiography predicting inflammation status around atherosclerotic plaque: a retrospective cohort study

Kunlin Ye[a], Lingtao Zhang[a], Hao Zhou[a], Xukai Mo[a] and Changzheng Shi[a,b]

[a]Medical Imaging Center, The First Affiliated Hospital of Jinan University, Guangzhou, China;[b]Subingtian center for speed research and training/Guangdong Key Laboratory of speed capability research, School of physical education, Jinan University,Guangzhou, China

ABSTRACT

Objectives: This study expolored the relationship between perivascular adipose tissue (PVAT) radiomic features derived from coronary computed tomography angiography (CCTA) and the presence of coronary artery plaques. It aimed to determine whether PVAT radiomic could non-invasively assess vascular inflammation associated with plaque presence.

Methods: In this retrospective cohort study, data from patients undergoing coronary artery examination between May 2021 and December 2022 were analyzed. Demographics, clinical data, plaque location and stenosis severity were recorded. PVAT radiomic features were extracted using PyRadiomics with key features selected using Least Absolute Shrinkage and Selection Operator (LASSO) and recursive feature elimination (RFE) to create a radiomics signature (RadScore). Stepwise logistic regression identified clinical predictors. Predictive models (clinical, radiomics-based and combined) were constructed to differentiate plaque-containing segments from normal ones. The final model was presented as a nomogram and evaluated using calibration curves, ROC analysis and decision curve analysis.

Results: Analysis included 208 coronary segments from 102 patients. The RadScore achieved an Area Under the Curve (AUC) of 0.897 (95% CI: 0.88–0.92) in the training set and 0.717 (95% CI: 0.63–0.81) in the validation set. The combined model (RadScore + Clinic) demonstrated improved performance with an AUC of 0.783 (95% CI: 0.69–0.87) in the validation set and 0.903 (95% CI: 0.83–0.98) in an independent test set. Both RadScore and combined models significantly outperformed the clinical model ($p < .001$). The nomogram integrating clinical and radiomics features showed robust calibration and discrimination (c-index: 0.825 in training, 0.907 in testing).

Conclusion: CCTA-based PVAT radiomics effectively distinguished coronary artery segments with and without plaques. The combined model and nomogram demostrated clinical utility, offering a novel approach for early diagnosis and risk stratification in coronary heart disease.

GRAPHICAL ABSTRACT

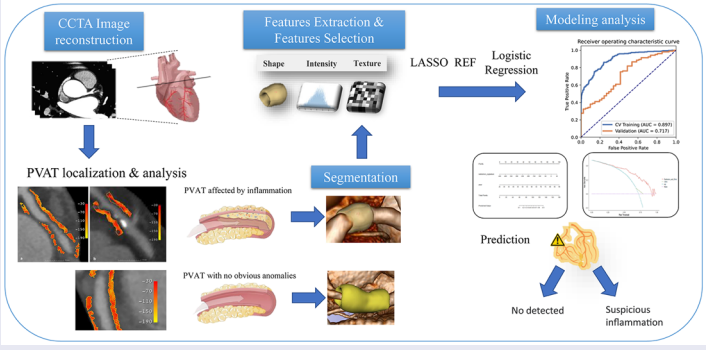

ARTICLE HISTORY

Received 15 May 2024
Revised 23 October 2024
Accepted 24 October 2024

KEYWORDS

Coronary computed tomography angiography; radiomics; fat attenuation index; coronary atherosclerotic plaque progression

CONTACT Changzheng Shi sczcn@126.com Medical Imaging Center, The First Affiliated Hospital of Jinan University, No. 613 West Huangpu Avenue, Tianhe District, Guangzhou 510630, China; Xukai Mo xukaimo@jnu.edu.cn Medical Imaging Center, The First Affiliated Hospital of Jinan University, No. 613 West Huangpu Avenue, Tianhe District, Guangzhou 510630, China
Kunlin Ye, Lingtao Zhang, and Hao Zhou contributed equally to this work.

© 2024 The Author(s). Published by Informa UK Limited, trading as Taylor & Francis Group
This is an Open Access article distributed under the terms of the Creative Commons Attribution-NonCommercial License (http://creativecommons.org/licenses/by-nc/4.0/), which permits unrestricted non-commercial use, distribution, and reproduction in any medium, provided the original work is properly cited. The terms on which this article has been published allow the posting of the Accepted Manuscript in a repository by the author(s) or with their consent.

Introduction

Although Global Cardiovascular diseases (CVDs) mortality rates varied, CVD have emerged as a significant global health concern, with approximately 19.1 million deaths recorded in 2020 [1]. One of the leading causes of CVD-related deaths is arteriosclerosis [2].

An inflammatory disease, atherosclerosis involves the deposition of lipids and macrophages within arterial walls [3]. The presence of inflammatory mediators in atherosclerotic plaques is associated with the pathogenesis of cardiovascular diseases, as these mediators regulate tissue factor expression and activate the atheroma macrophages [4–6].

Perivascular adipose tissue (PVAT) is a specialized type of adipose tissue that surrounds blood vessels, exerting both local and systemic effects [7]. Growing evidence supports the notion that the metabolic processes of PVAT contribute to endothelial dysfunction, inflammatory response and smooth muscle cell proliferation, thereby exerting influence on the initiation and progression of atherosclerotic plaques [8–10].

The metabolic crosstalk between PVAT and the arterial wall plays a pivotal role in atherosclerosis development [11]. PVAT-derived bioactive molecules and adipokines can directly modulate the inflammatory milieu within the vascular wall and the adjacent perivascular region, activating endothelial cells and promoting leukocyte recruitment [12,13]. Moreover, PVAT-induced dysregulation of lipid metabolism and adipose-derived cytokines may indirectly impact the arterial wall by promoting oxidative stress and altering the function of vascular endothelial cells, smooth muscle cells and macrophages [9,10,12,14].Understanding the intricate interplay between PVAT and atherosclerosis is of paramount importance for unravelling the underlying mechanisms and identifying novel therapeutic targets.

Identification and classification of coronary computed tomography angiography (CCTA) features for screening abnormal coronary is a crucial task in the field of cardiovascular medicine. With the advancements in medical imaging technology, specifically CCTA, it is now possible to detect and evaluate potential abnormalities in the coronary arteries non-invasively [11,15–17]. The perivascular fat attenuation index (FAI) focuses on the analysis of PVAT, have emerged as promising tools for assessing the prognostic significance of PVAT in predicting all-cause and cardiac mortality, surpassing the predictive capabilities of conventional clinical risk factors [18–21]. Previous research has placed considerable importance on assessing the inflammatory state of the pericoronary artery using non-invasive imaging techniques [7,22].

However, most existing studies focus on the association between PVAT and actual clinical outcomes [8,19–21,23,24], with limited exploration of quantitative indicators that can reflect functional differences in the vasculature. There is a notable gap in research comparing PVAT characteristics between vessels with and without coronary artery plaques. While non-invasive imaging techniques have been used to assess pericoronary inflammation, more precise and quantitative methods are needed to differentiate the inflammation status of different vascular segments. We hypothesize that there are differences in inflammation status between vessels with and without coronary artery plaques, which can be differentiated by PVAT radiomic features obtained from CCTA. Therefore, a retrospective analysis is being conducted to investigate the relationship between these radiomic features and abnormal PVAT status.

Methods and material

Patient characteristics

This retrospective study consecutively collected data on 183 patients who underwent coronary computed tomography angiography (CCTA) between May 2021 and December 2022 due to relevant examination indications. Based on the established criteria (Figure 1), 102 patients with a total of 208 coronary segments were included in the study. The patients were divided into two groups: those with coronary heart disease (CHD) and those without CHD. The study was reviewed and approved by the local medical ethics committee, and due to the retrospective nature of the study, the requirement for written informed consent was waived for all patients.

The inclusion criteria for patients with CHD were: (1) the presence of plaque or stenosis in the main branches of the coronary artery (left anterior descending branch, left circumflex branch and right coronary artery) as diagnosed by imaging, and (2) the diameter of the affected vessel segment was not less than 2 mm. The inclusion criteria for patients without CHD were those who underwent CCTA due to suspected coronary heart disease but with normal coronary arteries as diagnosed.

The common exclusion criteria were: (1) obvious respiratory and cardiovascular motion artefacts in the CCTA images; (2) incomplete CT data; (3) abnormal contrast enhancement in the coronary artery; (4) abnormalities, anomalies and variations in the

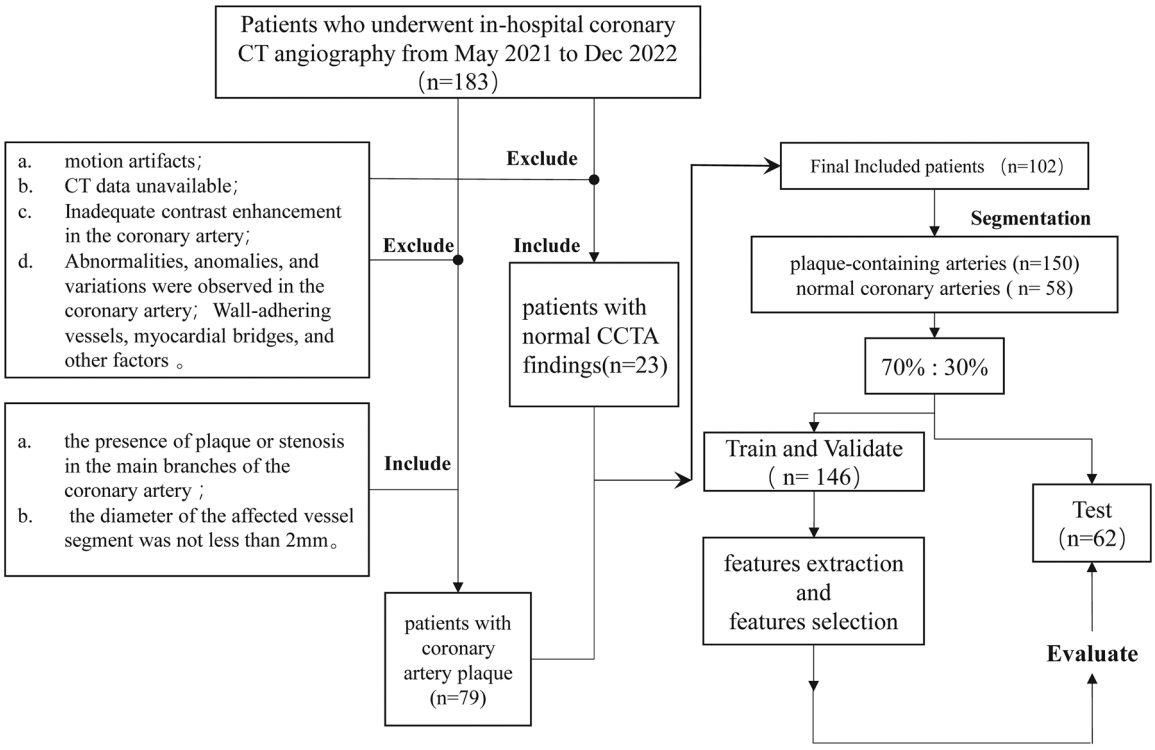

Figure 1. Flow chart showing case collection in the present study, with the inclusion and exclusion criteria.

coronary artery; (5) the presence of wall-adhering vessels or myocardial bridges.

The research protocol was approved by our institutional ethics committee. The experiment was conducted in accordance with guidelines and protocols relevant to clinical research, without any gender or racial disparities.

CCTA protocol and image reconstruction

All examinations were performed using a Toshiba Aquilion ONE 320-row CT scanner (Toshiba Medical Systems, Otawara, Japan). Prior to the examination, patients underwent breath-holding training at least 3 times to ensure stable inspiration amplitude. Patients with a heart rate ≥70 beats/min were administered 25–50 mg of metoprolol tartrate (Betaloc) orally 1 h before the examination to control the heart rate <70 beats/min and reduce motion artefacts.

The CCTA scanning range was set from 1 cm below the tracheal hilum to the lower edge of the cardiac diaphragm. A double-barrelled high-pressure injector was used to administer 50–70 mL of non-ionic iodinated contrast agent (iodopramide, iopamidol) and 40–50 mL of 0.9% saline solution into the antecubital vein, with an injection rate of 4.0–6.0 mL/s.

The contrast agent bolus tracking method was employed, with the threshold monitoring region of interest (ROI) set at the opening of the aorta. The default scan activation threshold was 100 HU. Monitoring began 10 s after contrast agent injection, and the CTA volume scan was automatically triggered when the ROI reached the threshold.

A prospective electrocardiogram triggering sequence was used for acquisition. For patients with a heart rate <70 beats/min, information was collected at 75% R-R interval, and for patients with a heart rate ≥75 beats/min, information was collected at 45% R-R interval. Automated tube voltage and current regulation technology was applied, with personalized settings determined for all patients based on their body mass index (BMI). The tube voltage was set at 100–120 kV (120 kV if BMI ≥25, 100 kV if BMI <25), tube current at 300–500 mA, layer thickness at 0.5 mm, matrix at 512 × 512 and gantry rotation time at 350 ms.

Semi-automated image analysis and segmentation

The target vessels included the left anterior descending (LAD), left circumflex (LCX) and right coronary artery (RCA). Two radiologists (with five and four years of cardiac imaging experience, respectively) evaluated each vessel independently without knowledge of clinical results.

The CCTA images were analysed using cvi42 software (version 5.1.1, Circle Cardiovascular Imaging Inc., Calgary, Alberta, Canada) to record the location and severity of the diseased vessels. The degree of stenosis was automated measured in cvi42, which employs the Minimum Lumen Area (MLA) method. This method automatically calculates the cross-sectional area of the lumen at the point of maximum stenosis and compares it to a reference lumen area to determine the percentage of stenosis. Using the open-source software 3D Slicer (version 5.0.3, www.slicer.org), the Voxels of interest (VOI) were drawn around the PVAT surrounding the vessel segments where the plaques were located, as compared to cvi42.

To ensure the accuracy and reproducibility of the PVAT VOI in vessel segments with plaques, another radiologist performed a second delineation. To further evaluate the inter-observer reproducibility of the VOI delineation, 20 randomly selected cases were used for intraclass correlation coefficient (ICC) analysis between the two radiologists. Any disagreements in VOI range were discussed and modified by the two radiologists to reach a consensus.

Feature extraction, selection and model development

Radiomic features were extracted using the PyRadiomics (github.com/radiomics/PyRadiomics) package in Python (version 3.6.13, www.python.org), after normalizing and resampling the CT images with a bin width of 100, normalized scale of 160 and resampled pixel spacing of ($0.2 \times 0.2 \times 0.2$ mm).

Radiomic features' categories are consistent with previously established standards [25]. These features can be categorized into several classes: First-order statistics describe the distribution of voxel intensities; Shape-based features describe the three-dimensional size and shape; Texture features capture spatial relationships between voxels and describe patterns or repeating elements, including features derived from various matrices such as gray level co-occurrence matrix (GLCM), gray level run length matrix (GLRLM) and gray level size zone matrix (GLSZM); and Higher-order statistics are obtained by applying mathematical transformations(wavelets) to the original image before extracting texture features.

The extracted radiomics features were randomly divided into a training-validation set and a testing set (70% and 30%, respectively). The training-validation set was utilized for model development and feature selection, while the test dataset was solely employed for the final testing of the model.

Z-Score was used to normalize all the radiomic features. To address the significant imbalance between non-plaque and plaque-containing artery groups, we employed the Synthetic Minority Oversampling Technique (SMOTE) [24,26]. SMOTE creates synthetic examples in the minority class by interpolating between existing minority instances, effectively balancing the dataset and mitigating the risk of model bias towards the majority class [24,26]. The feature matrix was further normalized, and before feature selection, we used Least Absolute Shrinkage and Selection Operator (LASSO) to perform dimensionality reduction on the data [27]. This can reduce the complexity of the model and the risk of overfitting, while improving the model's generalization ability [28].

For model construction, we utilized both clinical and radiomics features. Clinical features were derived from demographic, clinical and detailed coronary examination data collected for each patient. Radiomics features were extracted from the pericoronary adipose tissue of both plaque-containing and plaque-free coronary artery segments using PyRadiomics, resulting in an initial set of 851 potential features.

To identify the most relevant predictors, clinical features were selected through stepwise logistic regression, while radiomics features underwent a selection process combining LASSO and RFE with logistic regression as the classifier. Logistic regression, a linear classifier that combines all features, was chosen for its interpretability and effectiveness in binary classification problems [29].

Based on the clinical characteristics and radiomics features, we constructed three models: the Clinic model, radiomics-based model (RadScore model) and the combined model (RadScore + Clinic model).

To optimize each model's hyper-parameters, including the number of features, we employed five-fold cross-validation on the training and validation dataset [30]. This process ensured robust model performance and reduced the risk of overfitting.

The entire modelling process, including data processing and standardization, dataset partitioning, feature selection and model construction and validation, was conducted using Python with the scikit-learn package (version 0.24, scikit-learn.org/stable/) and FeAture Explorer Pro (FAE, V 0.5.5).

We developed a nomogram based on the logistic regression model to predict the probability of abnormal PVAT in specific sites of coronary arteries, integrating their clinical characteristics and radiomic features (Figure 6). This nomogram enhances the interpretability of the combined model by providing a visual representation of the contribution of each

selected feature to the prediction outcome. To assess model calibration and clinical utility, we generated calibration curves and decision curves for the models. The concordance index (c-index) was calculated for the nomogram in both training and testing datasets to assess discriminative ability using R software (version 4.1.3, www.R-project.org).

Statistical analysis

Statistical analysis employed T-test, ANOVA, Chi-square and Fisher's exact tests as appropriate for comparing demographic, clinical and radiomics features between plaque-containing and plaque-free coronary artery segments.

All statistical analyses were performed using R and Python. Continuous variables were reported as mean ± standard deviation (SD), while categorical variables were expressed as count and percentage. The Shapiro-Wilk test was used to assess the normality of the data distribution.

For comparing clinical characteristics and radiomics features between plaques, we employed the Student's t-test or Mann-Whitney U-test for quantitative variables, depending on the normality of distribution. The chi-square test or Fisher's exact test was used for categorical variables, as appropriate.

To evaluate the models' ability to distinguish coronary artery disease between patients, we conducted Receiver Operating Characteristic (ROC) curve analysis. We calculated the Area Under the Curve (AUC), accuracy, sensitivity and specificity at the cut-off value that maximized the Youden index. A 95% confidence interval (95%CI) for these metrics was estimated using bootstrapping with 1000 resamples.

The statistical significance level was set at $p < .05$ for all analyses. All tests were two-tailed, and the results were reported with their corresponding p values to allow for a comprehensive interpretation of the findings.

Results

Plaque-based characteristics

A total of 208 coronary segments from 102 patients were included in the study, comprising 150 (72.1%) segments from coronary plaque-containing arteries and 58 (27.9%) segments from normal coronary arteries. A statistically significant difference was observed in age ($p = .001$) between the two groups, with the coronary plaque group being older (57.01 ± 10.97 years) compared to the non-coronary plaque group (48.04 ± 10.66 years). No significant differences were found in gender, BMI, heart rate, hypertension, diabetes and hyperlipidaemia between the two groups (Table 1).

Table 1. Patients characteristics.

Variable	Category	Non-coronary plaque group ($n = 23$, 22.5%)	Coronary plaque group ($n = 79$, 77.5%)	p
Sex (n, %)	Male	16 (69.6)	46 (58.2)	.461
	Female	7 (30.4)	33 (41.8)	
Age(years)		48.04 (10.66)	57.01 (10.97)	.001*
BMI(kg/m^2)		23.53 (2.77)	24.86 (3.52)	.098
Heart rate(bpm)		72.65 (8.17)	69.56 (9.35)	.154
Hypertension (n, %)		4 (17.4)	11 (13.9)	.937
Diabetes (n, %)		2 (8.7)	3 (3.8)	.683
Hyperlipidaemia (n, %)		0 (0.0)	15 (19.0)	.054

Note: Data were expressed as means ± SD for continuous variables and number (percentage) for dichotomous variables. *P value of less than 0.05 was considered statistically significant.

Table 2. Plaque-based vessel segments characteristics.

Variable	Category	Non-plaque vessel segments ($n = 58$, 27.9%)	Plaque vessel segments ($n = 150$, 72.1%)	p
Vessel (n, %)	LAD	31 (53.4)	81 (54.0)	.743
	LCX	10 (17.2)	20 (13.3)	
	RCA	17 (29.3)	49 (32.7)	
Stenosis degree (n, %)	≤25%	58 (100.0)	14 (9.3)	<.001*
	26%~50%	0 (0.0)	102 (68.0)	
	51%~75%	0 (0.0)	23 (15.3)	
	≥76%	0 (0.0)	11 (7.3)	

Notes: Data were expressed as means ± SD for continuous variables and number (percentage) for dichotomous variables. LAD: left anterior descending artery; LCX: left circumflex artery; RCA: right coronary artery. *P value of less than 0.05 was considered statistically significant.

Regarding the distribution of coronary artery segments included in the study (Table 2), there were no significant differences between the plaque-containing and non-plaque groups ($p = .743$). The left anterior descending artery (LAD) was the most represented in both groups (54.0% of plaque segments and 53.4% of non-plaque segments), followed by the right coronary artery (RCA) (32.7% and 29.3%, respectively) and the left circumflex artery (LCX) (13.3% and 17.2%, respectively). As expected, there was a significant difference in the degree of stenosis between the plaque-containing and normal coronary artery segments ($p < .001$).

Radiomics assessment of the PVAT

Our initial radiomics analysis extracted 851 features from each Voxel of interest in both the training and testing sets, using original and wavelet-transformed images. Through LASSO and RFE feature selection methods applied to the training dataset, we identified 12 key features for logistic regression modelling (Figure 2, Table 3). Most of the features show good consistency (ICC > 0.9), except for wavelet-HHL_glszm_ZoneEntropy (ICC = 0.48). Despite some features having lower ICC values, we

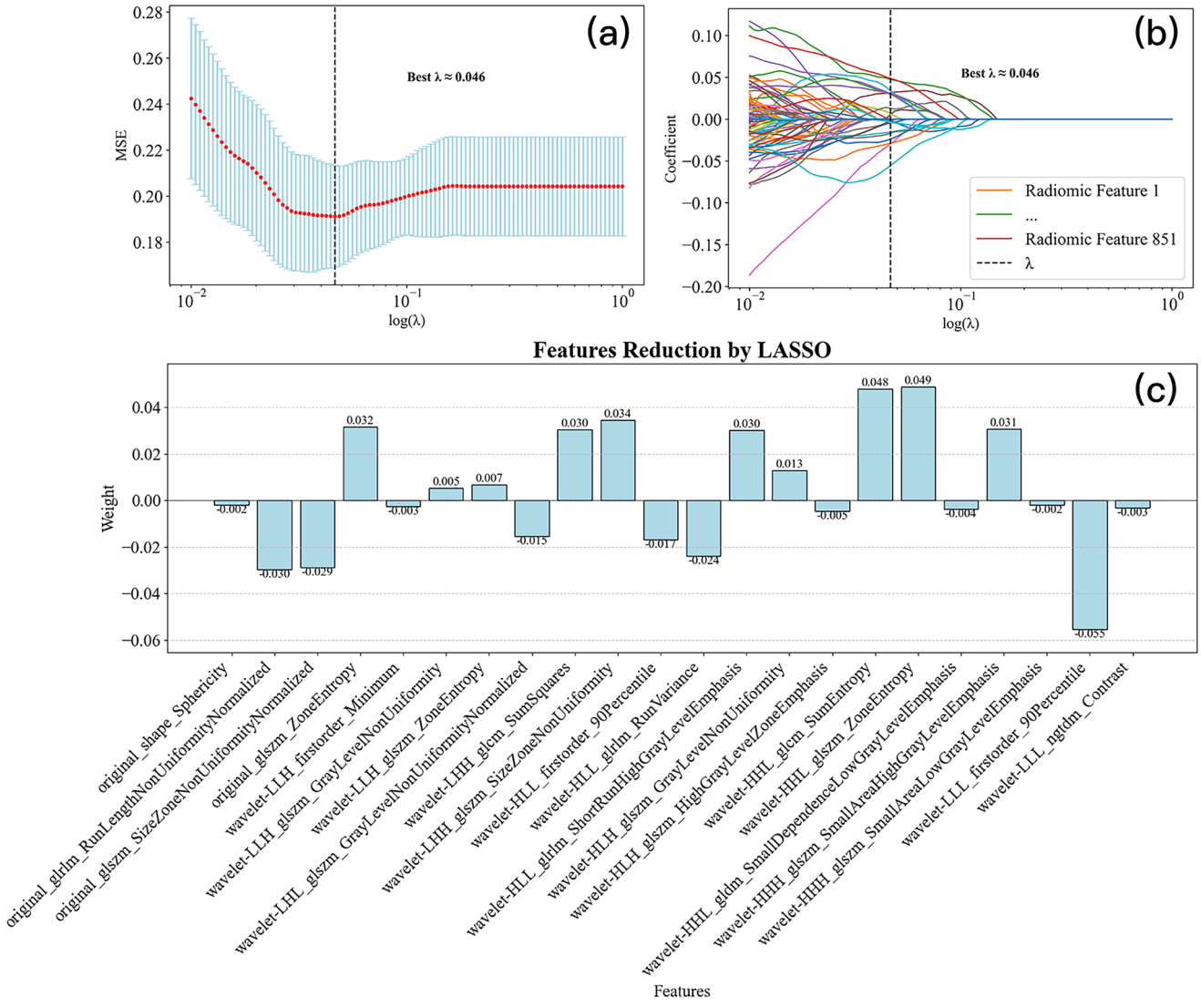

Figure 2. (a) LASSO regularization path, the optimal adjustment parameter λ was determined using the LASSO method through 10-fold cross-validation. (b) LASSO coefficient path for 829 imaging features. (c) The top 22 features after LASSO features selection.

Table 3. 12 Features finally selected for logistic regression modelling.

Selected features	Coefficients	ICC	95% CI
Original_shape_Sphericity	0.038	0.959	0.912 ~ 0.982
Original_glszm_SizeZoneNonUniformityNormalized	0.335	0.930	0.850 ~ 0.968
Original_glszm_ZoneEntropy	0.504	0.973	0.941 ~ 0.988
Wavelet-LLH_firstorder_Minimum	0.550	0.978	0.952 ~ 0.990
Wavelet-LLH_glszm_GrayLevelNonUniformity	0.766	0.925	0.841 ~ 0.966
Wavelet-LHH_glszm_SizeZoneNonUniformity	0.503	0.932	0.855 ~ 0.969
Wavelet-HLL_glrlm_ShortRunHighGrayLevelEmphasis	0.276	0.944	0.878 ~ 0.974
Wavelet-HLH_glszm_GrayLevelNonUniformity	0.616	0.932	0.854 ~ 0.969
Wavelet-HHL_glcm_SumEntropy	0.567	0.997	0.992 ~ 0.998
Wavelet-HHL_glszm_ZoneEntropy	0.322	0.480	0.121 ~ 0.728
Wavelet-HHH_glszm_SmallAreaHighGrayLevelEmphasis	0.153	0.743	0.506 ~ 0.876
Wavelet-LLL_firstorder_90Percentile	0.568	0.997	0.994 ~ 0.999
Intercept	0.290	–	–

retained them due to their potential clinical value, possible synergistic effects with other features and to maintain methodological diversity in this exploratory study.

Based on the logistic regression coefficients and intercept (Table 3), we constructed a radiomics signature (RadScore) as follows:

RadScore =

0.038 x original_shape_Sphericity − 0.335 x original_glszm_SizeZoneNonUniformityNormalized +

0.504 x original_glszm_ZoneEntropy − 0.550 x wavelet-LLH_firstorder_Minimum +

0.766 x wavelet-LLH_glszm_GrayLevelNonUniformity + 0.503 x wavelet-LHH_glszm_SizeZoneNonUniformity + 0.276 x wavelet-HLL_glrlm_ShortRunHighGrayLevel Emphasis +

0.616 x wavelet-HLH_glszm_GrayLevelNonUniformity + 0.567 x wavelet-HHL_glcm_SumEntropy +

0.322 x wavelet-HHL_glszm_ZoneEntropy +

0.153 x wavelet-HHH_glszm_SmallAreaHighGrayLevel Emphasis−

0.568 x wavelet-LLL_firstorder_90Percentile + 0.290

By using stepwise regression, we selected the variable of Age and combined it with the RadScore to construct a combined model.

Validation of the predictive model

Based on selected features, we finally constructed three models: the Clinic model (using selected clinical features), the radiomics-based model (RadScore model, using the 12 selected radiomics features) and the combined model (RadScore + Clinic model, incorporating both selected clinical and radiomics features).

All models underwent five-fold cross-validation. The RadScore model demonstrated moderate discriminatory ability with an AUC of 0.897 (95% CI: 0.88–0.92) for the cross-validation training set and 0.717 (95% CI: 0.63–0.81) for the validation set. In the validation set, it showed desirable sensitivity (75.2%) and specificity (58.5%). Notably, the RadScore + Clinic model demonstrated superior stability compared to the other models. This stability was evidenced by the closer alignment of its training and validation set ROC curves, a smaller gap between training and validation AUCs (0.844 vs. 0.783) and consistent curve shapes across both datasets. These characteristics suggest better generalization ability and more reliable performance across different data sets. In contrast, the Clinic model's performance was unsatisfactory, with an AUC of 0.520 (95% CI: 0.44–0.60). Both the RadScore and combined models significantly outperformed the Clinic model ($p < .001$, $z = 5.425$ and $p < .001$, $z = 6.570$, respectively). However, no statistically significant differences were observed between these two models' performances. Detailed results are presented in Table 4 and Figure 3.

We further evaluated the RadScore + Clinic model using an independent test dataset. This assessment demonstrated good discriminatory ability, with an AUC of 0.903 (95% CI: 0.83–0.98) (Figure 4).

Calibration curves were generated to evaluate the calibration of the two established models, which exhibited varying levels of performance. The calibration plot showed that the RadScore + Clinic model fit the observed data well, with the calibration curve aligning closely with the diagonal reference line indicating good calibration while the Clinic model's predictions appear less accurate, particularly for higher-risk predictions (Figure 5). We developed a nomogram based on logistic regression model to predict the probability of abnormal PVAT in specific site of coronary arteries, integrating their clinical characteristics and radiomic features (Figure 6). The nomogram demonstrated good performance in both training and testing datasets, with a c-index of 0.825 and 0.907, respectively.

We performed a decision curve analysis (DCA) to evaluate the net benefit of the clinic model and the combined model, showing the performance of both models across varying risk thresholds (Figure 7). The combined model demonstrates a higher net benefit over a wide range of risk thresholds from 0.05 to 0.75, significantly outperforming the clinic model alone ($p < .05$ across most thresholds). This indicates that the combined model provides greater clinical net benefit

Table 4. Performance of three different models.

Model	Cohort	AUC [95%CI]	Sensitivity [95%CI]	Specificity [95%CI]	Accuracy [95%CI]	Youden index [95%CI]
RadScore model	CV Training	0.897 [0.877–0.918]	0.862 [0.836–0.888]	0.76 [0.734–0.786]	0.811 [0.785–0.837]	0.621 [0.585–0.657]
	Validation	0.717 [0.644–0.790]	0.752 [0.726–0.778]	0.585 [0.559–0.611]	0.706 [0.680–0.732]	0.585 [0.549–0.621]
RadScore + Clinic model	CV Training	0.844 [0.819–0.868]	0.774 [0.747–0.801]	0.757 [0.730–0.784]	0.766 [0.739–0.793]	0.531 [0.495–0.567]
	Validation	0.783 [0.716–0.849]	0.657 [0.631–0.683]	0.854 [0.827–0.881]	0.712 [0.685–0.739]	0.511 [0.475–0.547]
Clinic model	CV Training	0.62 [0.588–0.652]	0.5 [0.474–0.526]	0.695 [0.668–0.722]	0.615 [0.588–0.642]	0.195 [0.159–0.231]
	Validation	0.52 [0.453–0.586]	0.422 [0.396–0.448]	0.688 [0.661–0.715]	0.578 [0.551–0.605]	0.11 [0.074–0.146]

Note: CV: cross validation; AUC: area under the curve; CI: confidence interval.

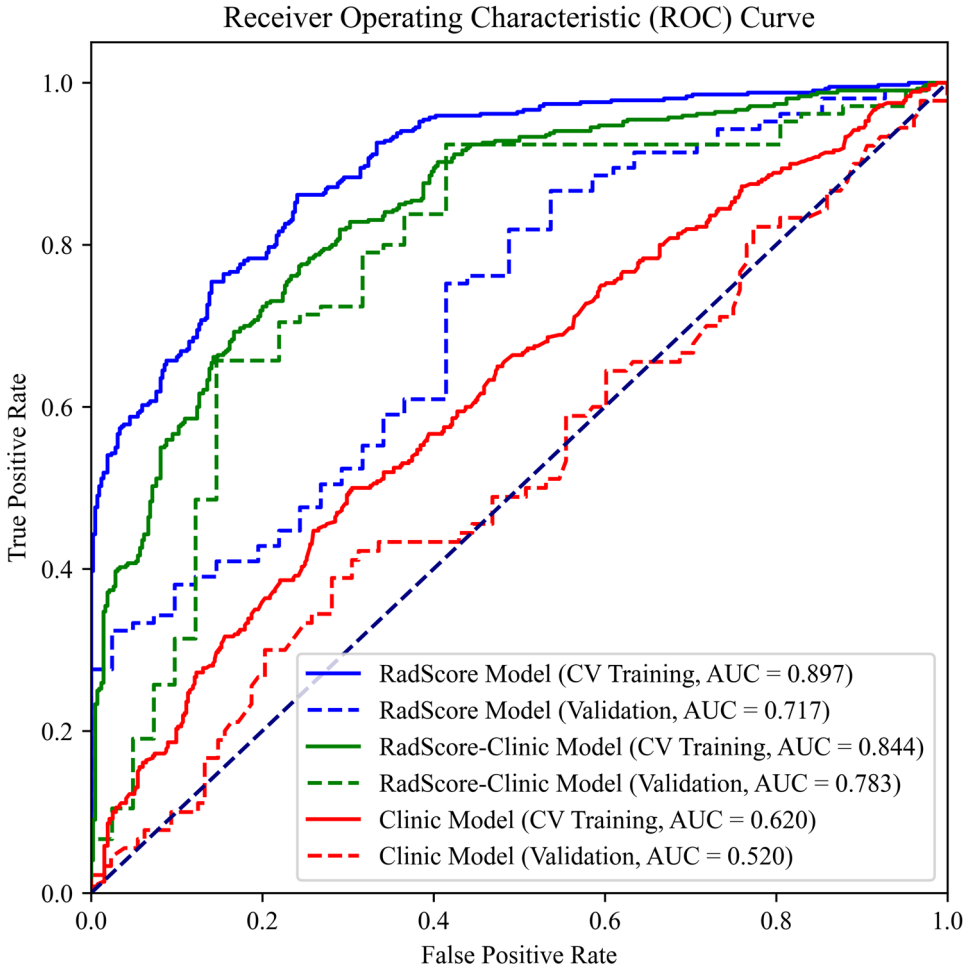

Figure 3. ROC curves depicting the performance of the RadScore, Clinic and RadScore + Clinic models in predicting abnormal PVAT status. The RadScore + Clinic model demonstrates superior stability, as evidenced by the closer alignment of its training (solid green line) and validation (dashed green line) set ROC curves.

when predicting inflammation status in vascular segments, indirectly reflecting the potential PVAT inflammation associated with plaques.

At risk thresholds below 0.05, the net benefit of both models is relatively close, with the clinic model slightly outperforming the combined model. However, as the risk threshold increases above 0.1, the combined model significantly outperforms the clinic model, and this trend continues up to a threshold of approximately 0.75. Beyond this point, the difference in net benefit narrows and approaches zero, with the combined model occasionally performing slightly worse than both the 'All' and 'None' strategies.

Discussion

This study demonstrated that models based on PVAT radiomics features could effectively differentiate between coronary artery segments with and without plaques, supporting the hypothesis that PVAT radiomic features can distinguish vascular inflammatory status associated with plaque presence. Our findings not only contributed to the growing body of evidence linking PVAT characteristics to CAD but also offered a novel perspective on the potential of radiomics in risk stratification and early detection of CAD.

The focus on comparing PVAT characteristics between vessel segments with and without plaques represents a shift from traditional approaches that primarily examine clinical outcomes in diagnosed CAD patients [9,31–35]. This paradigm shift allowed us to potentially capture the earliest stages of plaque formation, offering a window into the pathophysiological changes that precede clinically significant coronary artery disease [11]. Such early detection may have the potential to impact preventive cardiology, possibly enabling targeted interventions before the onset of symptomatic disease in some cases.

The superior performance of our RadScore model (AUC = 0.717, 95% CI: 0.63–0.81) compared to the clinical model underscores the potential of radiomics to capture subtle tissue changes that are not reflected in

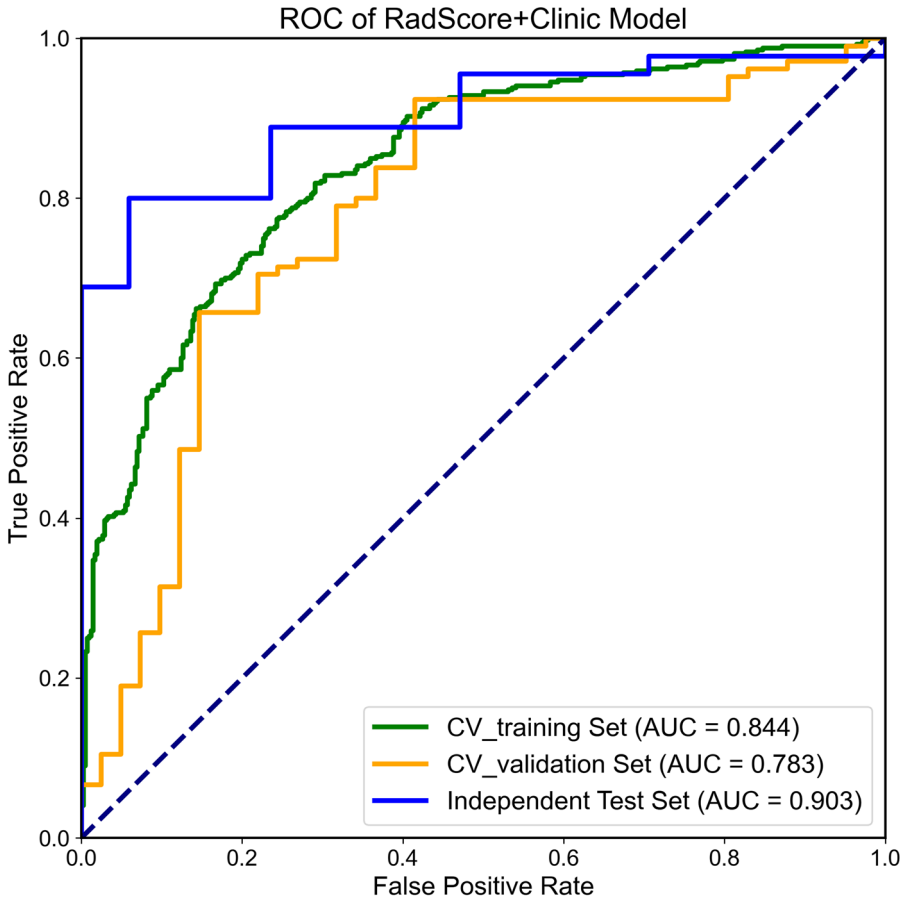

Figure 4. ROC curves of the RadScore + Clinic model for predicting abnormal PVAT status within the cross-validation training dataset, validation dataset and separate testing dataset.

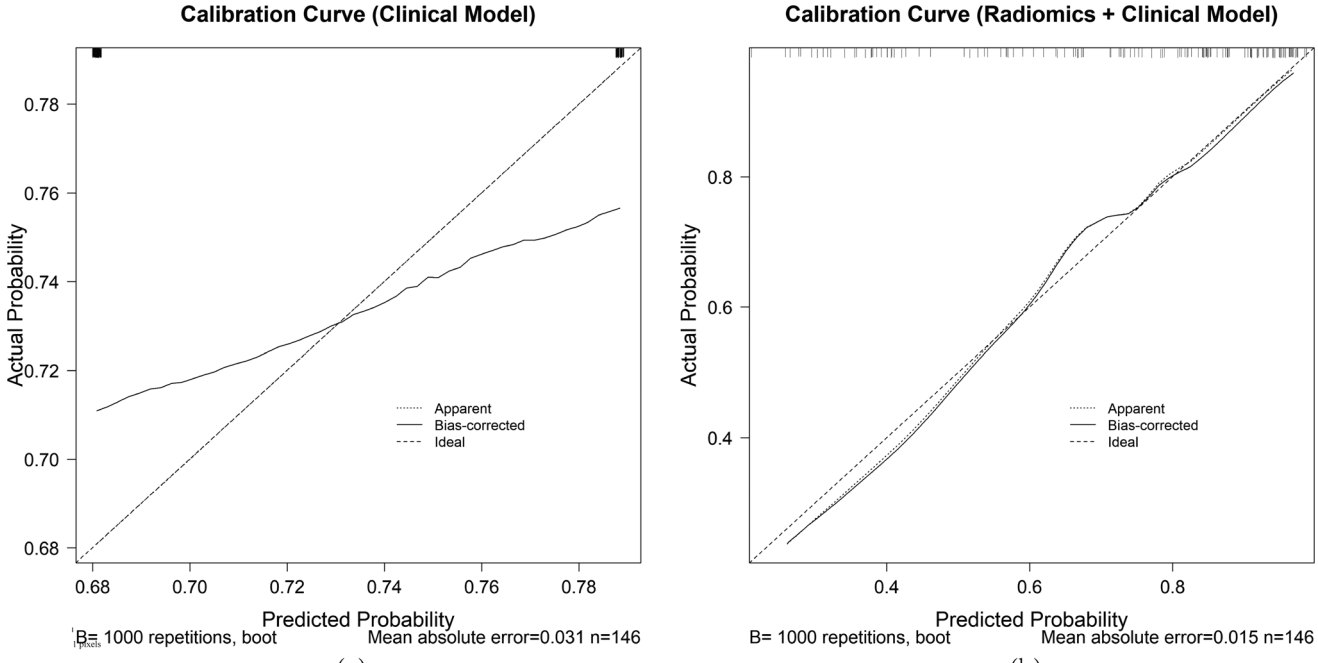

Figure 5. Calibration curves for the two predictive models: (a) Clinic model and (b) RadScore + Clinic model.

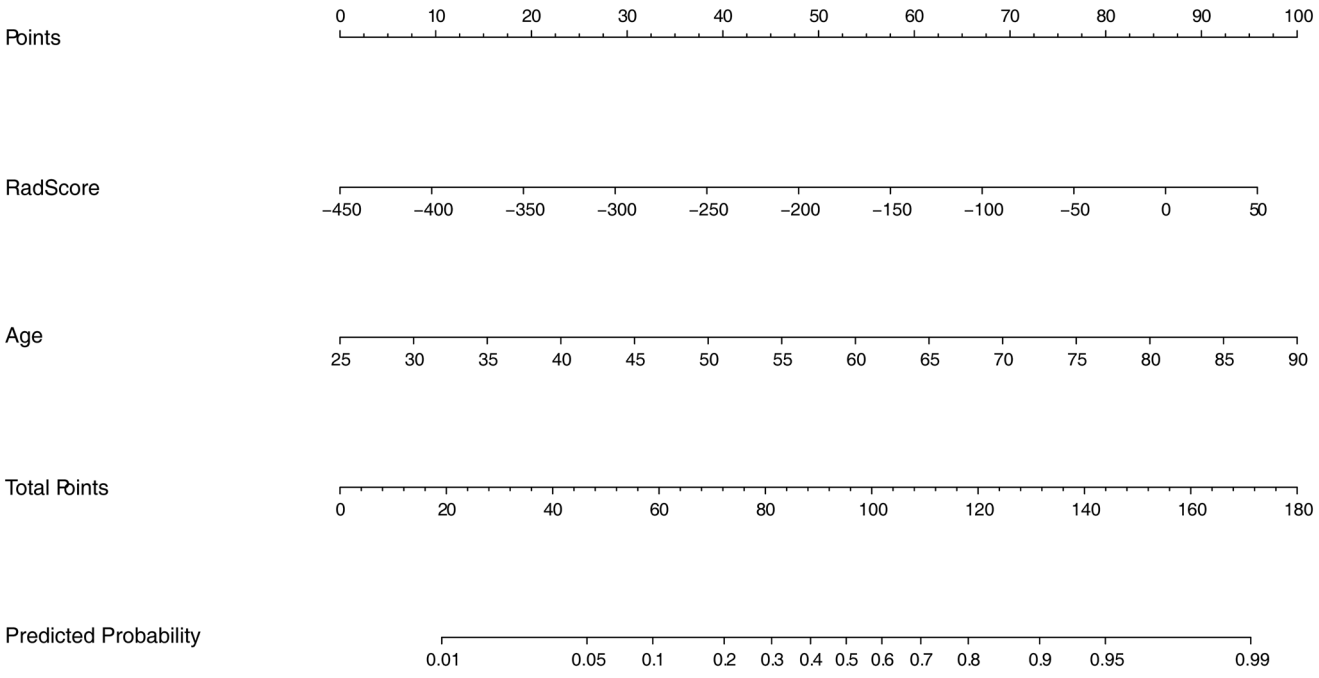

Figure 6. Nomogram for predicting abnormal PVAT status in specific site of coronary arteries.

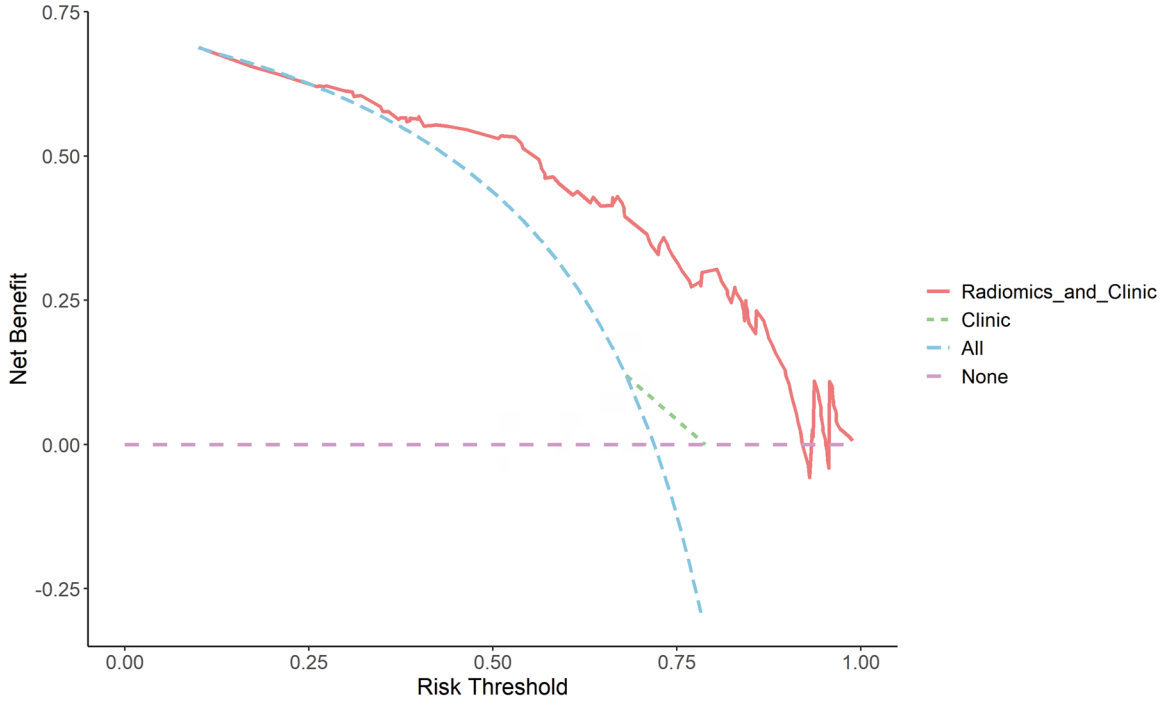

Figure 7. The decision curve analysis (DCA) of the clinic model and the combined model.

traditional risk factors [36]. This suggested that PVAT might undergo structural and functional alterations even before visible plaque formation, potentially serving as a 'canary in the coal mine' for coronary artery health. This finding was consistent with recent studies on the role of PVAT in the development of atherosclerosis [17,37], further supporting the notion that PVAT may be involved in coronary plaque formation. The integration of these radiomics features with clinical data in our combined model (AUC = 0.783, 95% CI: 0.69–0.87) further emphasized the synergistic potential of combining advanced imaging techniques with traditional clinical assessment.

Our final model retained some features with lower ICC values, such as wavelet-HHL_glszm_ZoneEntropy (ICC = 0.48). We chose to keep this feature in our

exploratory study despite its lower reproducibility, considering its potential to capture subtle tissue characteristics relevant to early atherosclerotic changes. However, we recognized the need for further validation in larger, more diverse cohorts to confirm its consistent contribution to model performance and to better understand its potential biological significance. This approach highlighted the exploratory nature of our study and emphasizes the importance of rigorous validation in future research.

Our decision curve analysis demonstrated the potential clinical utility of the combined model across a wide range of threshold probabilities. This suggested that the integration of PVAT radiomics into clinical decision-making could enhance risk stratification and potentially guide more targeted preventive strategies. However, the declining net benefit at very high threshold probabilities also highlighted the need for careful consideration of how such a model would be implemented in clinical practice.

The development of a nomogram based on our combined model represented a step towards translating complex radiomics data into a user-friendly tool for clinicians. This could potentially bridge the gap between advanced imaging analysis and practical clinical application, facilitating the integration of PVAT assessment into routine cardiovascular risk evaluation.

Our study provided a new approach for early identification of high-risk coronary artery segments. The differences in PVAT radiomics features may reflect different states of the tissue surrounding vessel segments with and without plaques, possibly related to local inflammation or metabolic changes [7,31]. Although our study could not directly prove that these changes predict future plaque formation, it laid the foundation for further research on the relationship between PVAT characteristics and plaque development.

This study has certain limitations. Firstly, the cross-sectional design limits our ability to establish causality between PVAT characteristics and plaque formation, suggesting a need for longitudinal studies. Secondly, our sample size, while sufficient for initial analysis, may not fully represent the variability in PVAT characteristics across a broader population. Consequently, external validation would be beneficial to assess model generalizability across different populations and imaging protocols, as suggested by previous research [34]. Furthermore, the complexity of radiomics features challenges biological interpretation, indicating a need for research linking computational features to specific PVAT pathological changes. Future studies addressing these aspects may help validate our findings and explore potential clinical applications of PVAT radiomics in coronary artery disease assessment.

Conclusion

In conclusion, our study demonstrated that CCTA-based PVAT radiomics analysis effectively differentiated between coronary artery segments with and without plaques, offering a novel approach for assessing local coronary artery status. This method may enhance early diagnosis and risk stratification of coronary heart disease. The developed nomogram, validated through decision curve analysis, shows potential as a clinical tool. While the specific role of PVAT characteristic differences in plaque formation requires further investigation, our findings pave the way for future studies, potentially advancing the understanding and prevention of coronary artery disease.

Ethical approval

This study has been approved by the Institutional Review Board of the First Affiliated Hospital of Jinan University (approval No. KY-2023-358) and has been performed in accordance with the Declaration of Helsinki.

Consent form

Institutional Review Board of the First Affiliated Hospital of Jinan University waived the consent to participate.

Author contributions

Kunlin Ye and Lingtao Zhang wrote the article; Hao Zhou analysed and interpreted the data; Xukai Mo and Changzheng Shi conceived and designed the experiments; Kunlin Ye and Lingtao Zhang performed the experiments. All authors reviewed the manuscript.

Disclosure statement

No potential conflict of interest was reported by the author(s).

Funding

This project was supported by the Guangzhou Science and Technology Project (2023A03J0609), Guangdong Province general university youth innovative talent project (2021KQNCX004), Guangdong Medical Science and Technology Research Foundation (A2021498), Scientific Research Program of Guangdong Provincial Bureau of Traditional Chinese Medicine (20222039) and The Fundamental Research Funds for the Central Universities (21624114 and 11620101).

Data availability statement

The data that support the findings of this study are available from the corresponding author, Xukai Mo, upon reasonable request.

References

[1] Tsao CW, Aday AW, Almarzooq ZI, et al. Heart disease and stroke statistics—2022 update: a report from the American Heart Association. Circulation. 2022;145(8):e153–e639. doi: 10.1161/CIR.0000000000001052.

[2] Kuller L. Sudden death in arteriosclerotic heart disease. Am J Cardiol. 1969;24(5):617–628. doi: 10.1016/0002-9149(69)90450-0.

[3] Ross R. Cell biology of atherosclerosis. Annu Rev Physiol. 1995;57(1):791–804. doi: 10.1146/annurev.ph.57.030195.004043.

[4] Ross R. Atherosclerosis—an inflammatory disease. Epstein FH, ed. N Engl J Med. 1999;340(2):115–126. doi: 10.1056/NEJM199901143400207.

[5] Lusis AJ. Atherosclerosis. Nature. 2000;407(6801):233–241. doi: 10.1038/35025203.

[6] Soehnlein O, Libby P. Targeting inflammation in atherosclerosis—from experimental insights to the clinic. Nat Rev Drug Discov. 2021;20(8):589–610. doi: 10.1038/s41573-021-00198-1.

[7] Antonopoulos AS, Sanna F, Sabharwal N, et al. Detecting human coronary inflammation by imaging perivascular fat. Sci Transl Med. 2017;9(398):eaal2658. doi: 10.1126/scitranslmed.aal2658.

[8] Hell MM, Achenbach S, Schuhbaeck A, et al. CT-based analysis of pericoronary adipose tissue density: relation to cardiovascular risk factors and epicardial adipose tissue volume. J Cardiovasc Comput Tomogr. 2016;10(1):52–60. doi: 10.1016/j.jcct.2015.07.011.

[9] Goeller M, Achenbach S, Cadet S, et al. Pericoronary adipose tissue computed tomography attenuation and high-risk plaque characteristics in acute coronary syndrome compared with stable coronary artery disease. JAMA Cardiol. 2018;3(9):858–863. doi: 10.1001/jamacardio.2018.1997.

[10] Tan N, Dey D, Marwick TH, et al. Pericoronary adipose tissue as a marker of cardiovascular risk. J Am Coll Cardiol. 2023;81(9):913–923. doi: 10.1016/j.jacc.2022.12.021.

[11] Lin A, Dey D, Wong DTL, et al. Perivascular adipose tissue and coronary atherosclerosis: from biology to imaging phenotyping. Curr Atheroscler Rep. 2019;21(12):47. doi: 10.1007/s11883-019-0817-3.

[12] Antonopoulos AS, Margaritis M, Verheule S, et al. Mutual regulation of epicardial adipose tissue and myocardial redox state by PPAR-γ/adiponectin signalling. Circ Res. 2016;118(5):842–855. doi: 10.1161/CIRCRESAHA.115.307856.

[13] Polkinghorne M, West H, Antoniades C. The role of perivascular fat in the diagnosis and prognosis of atherosclerosis. Cardiometab Syndr J. 2023;3(1):8. doi: 10.51789/cmsj.2023.3.e1.

[14] Margaritis M, Antonopoulos AS, Digby J, et al. Interactions between vascular wall and perivascular adipose tissue reveal novel roles for adiponectin in the regulation of endothelial nitric oxide synthase function in human vessels. Circulation. 2013;127(22):2209–2221. doi: 10.1161/CIRCULATIONAHA.112.001133.

[15] Mancio J, Oikonomou EK, Antoniades C. Perivascular adipose tissue and coronary atherosclerosis. Heart. 2018;104(20):1654–1662. doi: 10.1136/heartjnl-2017-312324.

[16] Kwiecinski J, Wolny R, Chwala A, et al. Advances in the assessment of coronary artery disease activity with PET/CT and CTA. Tomography. 2023;9(1):328–341. doi: 10.3390/tomography9010026.

[17] Zuo L, Tian Z, Zhou B, et al. Perivascular fat attenuation index value and plaque volume increased in non-target lesions of coronary arteries after stenting. Eur Radiol. 2024;34(7):4233–4242. doi: 10.1007/s00330-023-10468-8.

[18] Oikonomou EK, West HW, Antoniades C. Cardiac computed tomography: assessment of coronary inflammation and other plaque features. Arterioscler Thromb Vasc Biol. 2019;39(11):2207–2219. doi: 10.1161/ATVBAHA.119.312899.

[19] Lu G, Ye W, Ou J, et al. Coronary computed tomography angiography assessment of high-risk plaques in predicting acute coronary syndrome. Front Cardiovasc Med. 2021;8:743538. doi: 10.3389/fcvm.2021.743538.

[20] Klüner LV, Oikonomou EK, Antoniades C. Assessing cardiovascular risk by using the fat attenuation index in coronary CT angiography. Radiol Cardiothorac Imaging. 2021;3(1):e200563. doi: 10.1148/ryct.2021200563.

[21] Antoniades C, Antonopoulos AS, Deanfield J. Imaging residual inflammatory cardiovascular risk. Eur Heart J. 2020;41(6):748–758. doi: 10.1093/eurheartj/ehz474.

[22] Yamaura H, Otsuka K, Ishikawa H, et al. Determinants of non-calcified low-attenuation coronary plaque burden in patients without known coronary artery disease: a coronary CT angiography study. Front Cardiovasc Med. 2022;9:824470. doi: 10.3389/fcvm.2022.824470.

[23] Zhu X, Chen X, Ma S, et al. Dual-layer spectral detector CT to study the correlation between pericoronary adipose tissue and coronary artery stenosis. J Cardiothorac Surg. 2021;16(1):325. doi: 10.1186/s13019-021-01709-2.

[24] Oikonomou EK, Williams MC, Kotanidis CP, et al. A novel machine learning-derived radiotranscriptomic signature of perivascular fat improves cardiac risk prediction using coronary CT angiography. Eur Heart J. 2019;40(43):3529–3543. doi: 10.1093/eurheartj/ehz592.

[25] Zwanenburg A, Vallières M, Abdalah MA, et al. Image biomarker standardisation initiative. Radiology. 2020;295(2):328–338. doi: 10.1148/radiol.2020191145.

[26] Kotsiantis SB, Kanellopoulos D, Pintelas PE. Data preprocessing for supervised leaning. Int J Comput Sci. 2007;1(1):111–117. doi: 10.5281/zenodo.1082415.

[27] Tibshirani R. Regression shrinkage and selection via the lasso. J R Stat Soc B. 1996;58(1):267–288. doi: 10.1111/j.2517-6161.1996.tb02080.x.

[28] Candes E, Tao T. The Dantzig selector: statistical estimation when p is much larger than n. Ann Statist. 2007;35(6):2313–2351. doi: 10.1214/009053606000001523.

[29] Peng CYJ, Lee KL, Ingersoll GM. An introduction to logistic regression analysis and reporting. J Educ Res. 2002;96(1):3–14. doi: 10.1080/00220670209598786.

[30] Royston P, Moons KGM, Altman DG, et al. Prognosis and prognostic research: developing a prognostic model. BMJ. 2009;338(mar31 1):b604–b604. doi: 10.1136/bmj.b604.

[31] Oikonomou EK, Marwan M, Desai MY, et al. Non-invasive detection of coronary inflammation using computed tomography and prediction of residual cardiovascular risk (the CRISP CT study): a post-hoc analysis of pro-

spective outcome data. Lancet. 2018;392(10151):929–939. doi: 10.1016/s0140-6736(18)31114-0.

[32] Sagris MS, Antonopoulos AA, Simantiris SS, et al. Pericoronary adipose tissue attenuation index (FAI) – a new imaging biomarker and its diagnostic and prognostic utility: a systematic review and meta-analysis. ResearchGate. 2021;42(Supplement_1):ehab724.0197. doi: 10.1093/eurheartj/ehab724.0197.

[33] van der Bijl P, Kuneman JH, Bax JJ. Pericoronary adipose tissue attenuation: diagnostic and prognostic implications. Eur Heart J Cardiovasc Imaging. 2022;23(12):e537–e538. doi: 10.1093/ehjci/jeac175.

[34] Sagris M, Antonopoulos AS, Simantiris S, et al. Pericoronary fat attenuation index—a new imaging biomarker and its diagnostic and prognostic utility: a systematic review and meta-analysis. Eur Heart J Cardiovasc Imaging. 2022;23(12):e526–e536. doi: 10.1093/ehjci/jeac174.

[35] Chatterjee D, Shou BL, Matheson MB, et al. Perivascular fat attenuation for predicting adverse cardiac events in stable patients undergoing invasive coronary angiography. J Cardiovasc Comput Tomogr. 2022;16(6):483–490. doi: 10.1016/j.jcct.2022.05.004.

[36] Tsao CW, Aday AW, Almarzooq ZI, et al. Heart disease and stroke statistics—2023 update: a report from the American Heart Association. Circulation. 2023;147(8):e93–e621. doi: 10.1161/CIR.0000000000001123.

[37] Lee SE, Sung JM, Andreini D, et al. Association between changes in perivascular adipose tissue density and plaque progression. JACC Cardiovasc Imaging. 2022;15(10):1760–1767. doi: 10.1016/j.jcmg.2022.04.016.